Earth and Planetary Science Letters 447 (2016) 84–94

Contents lists available at ScienceDirect

Earth and Planetary Science Letters

www.elsevier.com/locate/epsl

Early degassing of lunar urKREEP by crust-breaching impact(s)

Jessica J. Barnes [a,*], Romain Tartèse [a,b], Mahesh Anand [a,c], Francis M. McCubbin [d], Clive R. Neal [e], Ian A. Franchi [a]

[a] Planetary & Space Sciences, The Open University, Walton Hall, MK7 6AA, UK
[b] Institut de Minéralogie, de Physique des Matériaux et de Cosmochimie, Muséum National d'Histoire Naturelle, Sorbonne Universités, CNRS, UPMC & IRD, 75005 Paris, France
[c] Earth Sciences department, Natural History Museum, London, SW7 5BD, UK
[d] NASA Johnson Space Center, Mailcode XI2, 2101 NASA Parkway, Houston, TX 77058, USA
[e] Department of Civil & Environmental Engineering & Earth Science, University of Notre Dame, IN 46556, USA

ARTICLE INFO

Article history:
Received 4 December 2015
Received in revised form 18 April 2016
Accepted 20 April 2016
Available online 13 May 2016
Editor: B. Marty

Keywords:
Moon
apatite
volatiles
NanoSIMS
chlorine
magma ocean

ABSTRACT

Current models for the Moon's formation have yet to fully account for the thermal evolution of the Moon in the presence of H_2O and other volatiles. Of particular importance is chlorine, since most lunar samples are characterised by unique heavy $\delta^{37}Cl$ values, significantly deviating from those of other planetary materials, including Earth, for which $\delta^{37}Cl$ values cluster around ~0‰. In order to unravel the cause(s) of the Moon's unique chlorine isotope signature, we performed a comprehensive study of high-precision *in situ* Cl isotope measurements of apatite from a suite of Apollo samples with a range of geochemical characteristics and petrologic types. The Cl-isotopic compositions measured in lunar apatite in the studied samples display a wide range of $\delta^{37}Cl$ values (reaching a maximum value of +36‰), which are positively correlated with the amount of potassium (K), Rare Earth Element (REE) and phosphorous (P) (KREEP) component in each sample. Using these new data, integrated with existing H-isotope data obtained for the same samples, we are able to place these findings in the context of the canonical lunar magma ocean (LMO) model. The results are consistent with the urKREEP reservoir being characterised by a $\delta^{37}Cl$ ~+30‰. Such a heavy Cl isotope signature requires metal-chloride degassing from a Cl-enriched urKREEP LMO residue, a process likely to have been triggered by at least one large crust-breaching impact event that facilitated the transport and exposure of urKREEP liquid to the lunar surface.

1. Introduction

Existing models for the formation of the Moon (Ćuk and Stewart, 2012; Canup, 2012) predict widespread melting and partial vaporisation of silicate material. Hydrodynamic escape (Pahlevan and Stevenson, 2007) may have facilitated the extensive loss of volatiles to the vacuum of space during the proto-lunar disk phase. Pahlevan and Stevenson (2007) also presented an elegant model to explain the isotopic similarity of oxygen isotopes (e.g., Wiechert et al., 2001) between the Earth and the Moon. In addition, Canup et al. (2015) have recently provided possible mechanisms to explain some isotopic differences between these two bodies (e.g., Zn). However, collectively these models have yet to fully reconcile the thermal evolution of the early Moon with the presence of H_2O and other associated volatile signatures in the lunar interior, that have been recognised through studies of lunar samples.

In lunar rocks, apatite [$Ca_5(PO_4)_3(F,Cl,OH)$] is the most common volatile-bearing mineral (McCubbin et al., 2015a). A multitude of studies have investigated the abundances of volatiles (H_2O, F, and Cl, e.g., McCubbin et al., 2010a, 2010b, 2011; Boyce et al., 2010) and the hydrogen isotopic compositions of lunar apatite (e.g., Greenwood et al., 2011; Barnes et al., 2013, 2014; Tartèse et al., 2013, 2014a, 2014b; Boyce et al., 2015). These studies have shown that (i) parental melts to the mare basalts contained H_2O > F > Cl, whilst the parent melts to the lunar highlands rocks were characterised by Cl > H_2O ≈ F (McCubbin et al., 2015a), and (ii) that apatite in mare basalts were generally characterised by elevated H-isotope signatures (>+600‰, Greenwood et al., 2011; Tartèse et al., 2013). These H-isotope compositions are similar to those measured in the lunar picritic glasses (Saal et al., 2013; Füri et al., 2014), which have been interpreted, at least in part, as resulting from degassing of molecular H_2 during ascent and emplacement of basaltic magmas on the lunar surface under reducing conditions. Currently, it has been argued that only a few samples (olivine-hosted melt inclusions trapped within picritic

* Corresponding author.
E-mail address: jessica.barnes@open.ac.uk (J.J. Barnes).

http://dx.doi.org/10.1016/j.epsl.2016.04.036

glass beads, some KREEP basalts and a few plutonic highlands rocks) may have preserved primitive lunar H-isotopic compositions (Saal et al., 2013; Barnes et al., 2014; Tartèse et al., 2014a). In the context of the lunar magma ocean (LMO) model, late-stage LMO residual melts are thought to have been enriched in incompatible elements such as K, REEs, and P, which are collectively called urKREEP or a KREEP-component, when referred to as a geochemical reservoir or geochemical component, respectively (Warren and Wasson, 1979). It is anticipated that chlorine (and other volatiles) should have been concentrated in the residual LMO melts given its incompatibility in olivine and pyroxene, which were the dominant early phases to crystallise in the cumulate pile of the LMO (e.g., Snyder et al., 1992; Elkins-Tanton et al., 2002, 2011; Elkins-Tanton and Grove, 2011; Elardo et al., 2011). When compared to chondritic meteorites and terrestrial rocks (e.g., Sharp et al., 2013a), most lunar samples have exotic Cl isotopic compositions (Sharp et al., 2010; Treiman et al., 2014; Tartèse et al., 2014b; Boyce et al., 2015), which are difficult to explain in light of the abundance and isotopic composition of other volatile species, especially H, and the current estimates for Cl and H_2O in the Bulk Silicate Moon (BSM) (Hauri et al., 2015; McCubbin et al., 2015a).

In order to fully understand the meaning and significance of the unique Cl-isotope compositions displayed by the majority of lunar rocks and to place these in the context of the differentiation of the Moon, we investigated the Cl-isotopic composition of apatite from a diverse set of lunar samples from Apollo missions: 11 (10044 & 10058), 14 (14304), 15 (15386 & 15555), and 17 (70035, 76535, 78235 & 79215). Our sample set covers a range of lunar lithological types, including KREEP and very high potassium (VHK) basalts, and selected plutonic highlands rocks (full details can be found in the Supplementary Information).

2. Analytical protocols

High-precision *in situ* measurements of Cl-isotopes and volatiles in apatite from the following nine Apollo thin-sections were carried out in this work: 10044,645; 10058,254; 14304,177; 15386,46; 15555,206; 70035,195; 76535,51; 78235,43 and 79215,50. Twenty eight apatite grains were identified as being suitable for analysis by ion probe (see below). During the analytical campaign, scanning electron microscopy (SEM) and electron probe microanalysis (EPMA) were carried out in order to characterise mineral chemistry in the thin-sections studied, following the methods detailed in Barnes et al. (2014).

The abundance and isotopic composition of Cl in lunar apatite grains were measured using the Cameca NanoSIMS 50L at the Open University and a protocol modified after Tartèse et al. (2014b) over three analytical campaigns from November 2014 to August 2015. Analyses were carried out using a Cs^+ primary beam of ~1 μm diameter, with an accelerating voltage of ~16 kV. Before each analysis, the area of interest was pre-sputtered using a ~120 pA probe current for 3 minutes at 8 × 8 μm to ensure the area was thoroughly cleaned of surface contamination. Analyses were performed using a primary probe current of between 40 and 60 pA, for ~5 minutes, over rastered areas of between 3 × 3 μm and 5 × 5 μm. Electronic gating was used to collect secondary ions emitted from only the inner 25% of the rastered areas. Secondary negative ions of $^{16}O^1H$, ^{18}O, ^{35}Cl, ^{37}Cl, and $^{40}Ca^{19}F$ were collected simultaneously on electron multipliers (EMs). $^{40}Ca^{19}F$ was used to easily identify apatite on real-time secondary ion images during pre-sputtering and to monitor F contents, but it was not used to precisely quantify apatite F contents due to the poor ionisation efficiency of $^{40}Ca^{19}F$. A mass resolving power of ~8000 (Cameca definition) was used in order to readily resolve isobaric interferences, particularly between peaks of ^{17}O and $^{16}O^1H$. Each 1-inch round thin-section was coated with ~30 nm of gold and an electron flood gun was used for charge compensation. Secondary ion images of $^{16}O^1H$ were monitored in real time during pre-sputtering and after analysis to ensure that the analysed areas were free of any surficial contamination, cracks, or hotspots.

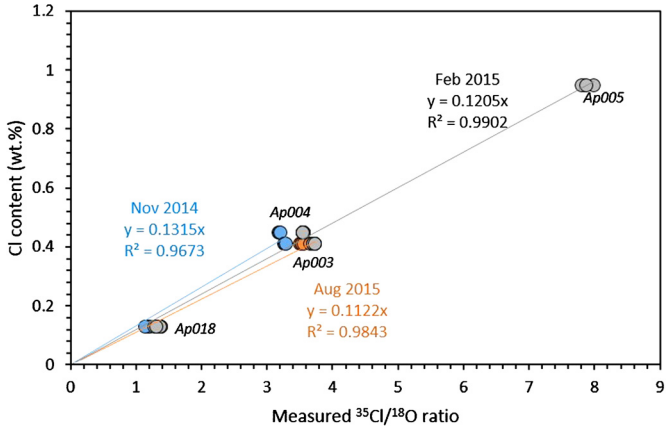

Fig. 1. Calibrations for the apatite standards used in this study of known Cl content (wt%) versus the measured $^{35}Cl/^{18}O$ ratio, for a representative analytical day during each of the three analytical sessions.

Apatite Cl contents were calibrated using the measured $^{35}Cl/^{18}O$ ratios and the known Cl contents of terrestrial apatite standards (described in McCubbin et al., 2010a, 2012), which were pressed into an indium mount along with a San Carlos olivine crystal that was used to estimate background abundances of H_2O (between ~10 and 90 ppm) and Cl (<5 ppm). The slopes of the calibration lines (Fig. 1) defined by apatite standards with varying Cl contents were used to calculate the Cl contents of apatite in the Apollo samples. The uncertainties reported on the Cl contents of the 'unknown' apatite combine the 2σ uncertainty associated with the calibrations and the analytical uncertainties associated with each individual measurement.

Finally, two of the reference apatite grains, Ap005 or Ap004 (McCubbin et al., 2012), were used to correct the measured $^{37}Cl/^{35}Cl$ ratios for instrumental mass fractionation. The isotopic composition of chlorine is reported using the standard delta (δ) notation with respect to the $^{37}Cl/^{35}Cl$ ratio of the standard mean ocean chloride (SMOC, $^{37}Cl/^{35}Cl$ ratio = 0.31977), and is reported with the associated 2σ uncertainties, which combine the reproducibility of $^{37}Cl/^{35}Cl$ measurements on the reference apatite (either Ap005 or Ap004) and the internal uncertainty of each analysis. Fig. 2 shows an example of the reproducibility of $\delta^{37}Cl$ values measured on a secondary apatite standard (Ap003) run during the February session and referenced to Ap004 (Ap004 has a $\delta^{37}Cl$ value of ~+0.11‰, Zach Sharp, University of New Mexico, *pers. comm.*). All Ap003 analyses are within error of the terrestrial value of ~0 ± 1‰ (Sharp et al., 2013a), with an average $\delta^{37}Cl$ value for the analytical week of +0.17 ± 1.26‰.

3. Results

3.1. Petrographic context of lunar apatite

In thin-section 10044,645, apatite occurs in contact with non-mesostasis pyroxene, plagioclase and sometimes with troilite (apatite 5, for example, which is one of the largest apatite grains in this sample at ~200 μm in the longest dimension; Fig. 3A). Apatite also occurs enclosed, almost exclusively, within clinopyroxene crystals. For example apatite 6C, which is <50 μm in the longest dimension and is euhedral (showing basal section habit) on one side but displays a partially resorbed texture on the other side of

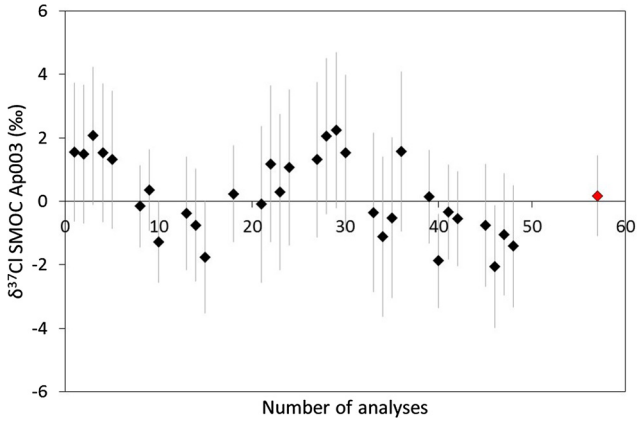

Fig. 2. Plot of δ^{37}Cl values for secondary apatite standard (Ap003) for analyses from 13th February to 18th February 2015. The error bars represent the 2σ uncertainties and are a combination of the reproducibility on the primary reference apatite and analytical error associated with individual measurements. The red diamond at the extreme right hand side of the plot, is the average δ^{37}Cl value for that session and the error bars represent the standard deviation of the measured values ($n = 32$). (For interpretation of the references to colour in this figure legend, the reader is referred to the web version of this article.)

the crystal (Fig. 3B). Apatite analysed in this study is also present in direct contact with mesostasis minerals, mostly K-feldspar, silica, fayalite, and a symplectite assemblage consisting of fayalite, silica, and Ca-rich pyroxene that is enclosed by plagioclase laths (e.g., the ~60 μm acicular apatite 6D in Fig. 3C). The majority of apatite in sample 10044 contain small <5 μm-sized inclusions of plagioclase, K-feldspar and occasionally, iron sulphide (troilite).

In thin-section 10058,254, apatite is commonly found in late-stage mesostasis areas comprised of K-rich phases (K-feldspar and occasionally K-rich glass), troilite, baddeleyite, pyroxene, silica, Fe-pyroxene, tranquillityite, ilmenite, fayalite, and a symplectite assemblage. We observed apatite in contact with either late-stage K-feldspar, silica and other phases (e.g., Fig. 3D) or in contact with plagioclase, pyroxene, and a symplectite assemblage (e.g., Fig. 3E). We did not observe a relationship between apatite crystal size and petrographic setting, and apatite occurs as subhedral hexagonal to tabular crystals of up to ~90 μm in length.

In thin-section 15555,206, apatite occurs enclosed in pyroxene (type 1) or, more commonly, in contact with plagioclase, pyroxene, silica, and K-feldspar (type 2). Apatite 1 analysed in this work is in the type 2 location (Fig. 3F) where it forms acicular rods of up to 100 μm in length. Apatite 5 also analysed here is found between type 1 and type 2 petrographic settings (Fig. 3G) where it

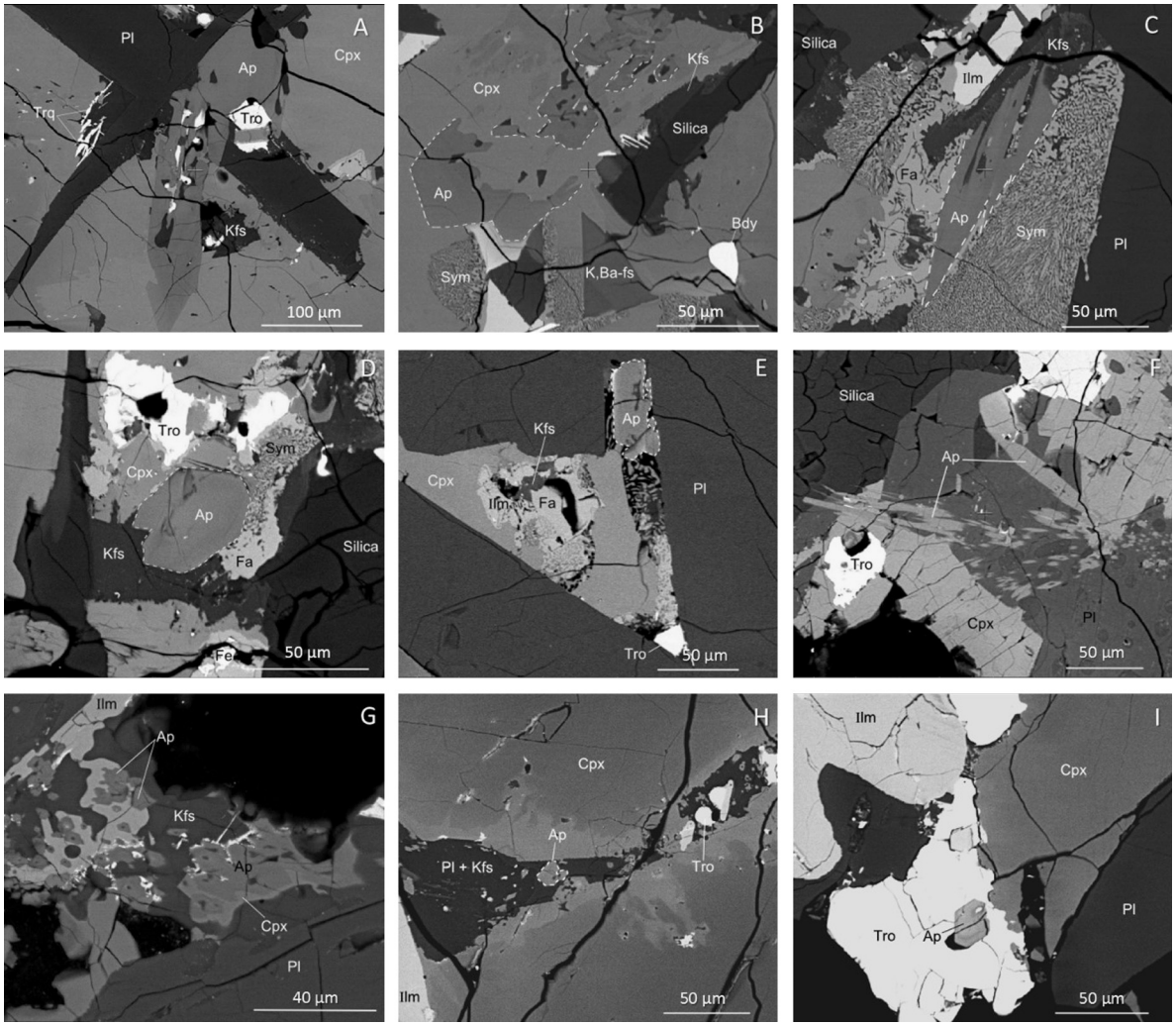

Fig. 3. Back-scattered electron (BSE) images of selected apatite crystals in the mare basalts studied: 10044,645; 10058,254; 15555,206 and 70035,195. A = 10044 apatite 5, B = 10044 apatite 6C, C = 10044 apatite 6D, D = 10058 apatite 5, E = 10058 apatite 6, F = 15555 apatite 1, G = 15555 apatite 5, H = 70035 apatite 15, and I = 70035 apatite 17. Where: Ap = apatite, Bdy = baddeleyite, Cpx = clinopyroxene, Kfs = potassium-rich (often Ba-rich) alkali feldspar, Fa = fayalite, Ilm = ilmenite, Pl = plagioclase, Sym = symplectite assemblage (Ca-rich pyroxene, fayalite, silica), Tro = troilite, and Trq = tranquillityite.

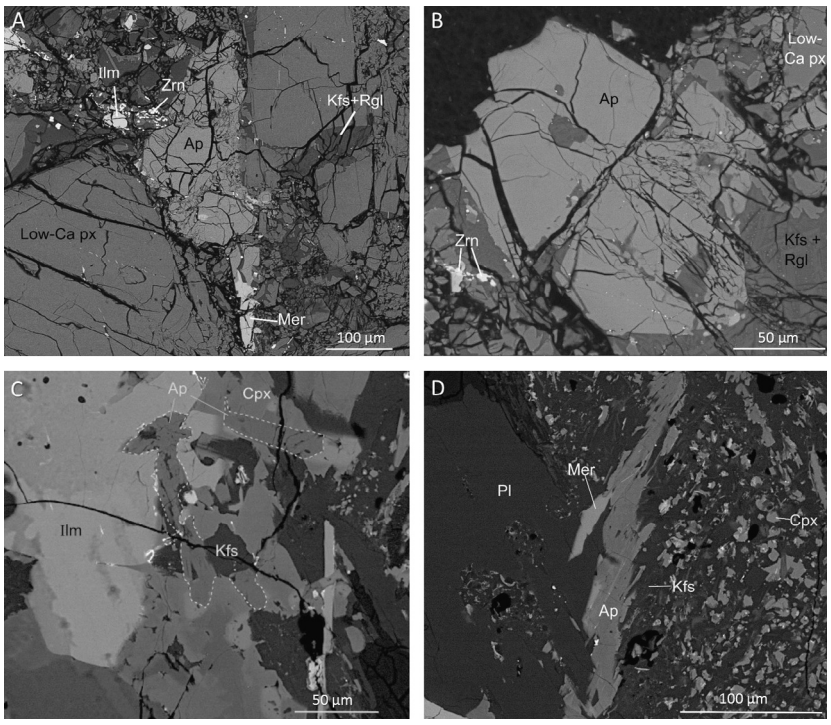

Fig. 4. BSE images of apatite crystals and their surrounding petrographic context in KREEP-rich basalts: 14304,177 and 15386,46. A = 14304 apatite 4, B = 14304 apatite 5, C = 15386 apatite 2, and D = 15386 apatite 5. Mineral abbreviations as in caption for Fig. 3, Mer = merrillite and Zrn = zircon, and Rgl = residual K-rich glass.

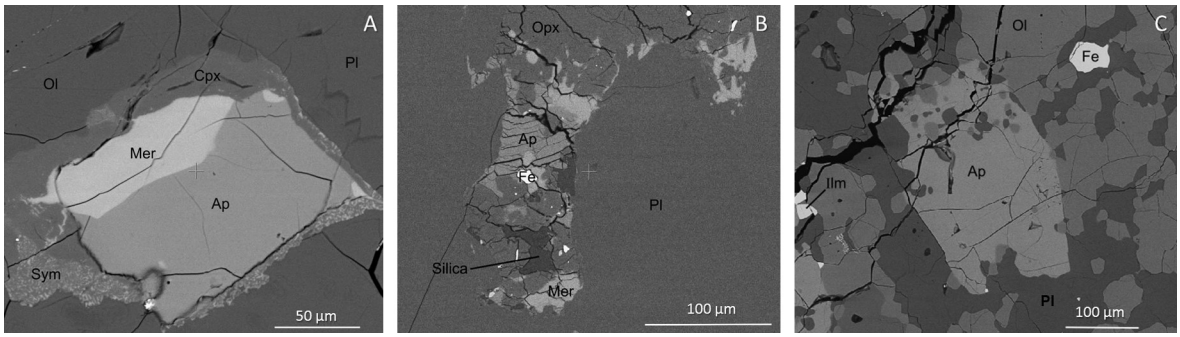

Fig. 5. BSE images showing the petrographic context of apatite in the highlands and the impact-related sample studied: 76535,51; 78235,43 and 79215,50. A = 76535 apatite 3, B = 78235 apatite 5, and C = 79215 apatite 12. Mineral abbreviations as in caption to Fig. 3, Opx = orthopyroxene, Ol = olivine, Fe = iron nickel blebs, and Sym = symplectite assemblage (Mg–Al chromite and two-pyroxenes, Elardo et al., 2012).

is most commonly enclosed in clinopyroxene as euhedral to subhedral crystals of up to ~30 µm in the longest dimension and typically containing plagioclase inclusions.

In thin-section 70035,195, apatite crystals 15 and 17 both occur as basal sections (hexagonal) of ~20 µm in diameter (Fig. 3H and 3I). Apatite in this section is very rare and occurs mostly in mesostasis areas in contact with K-feldspar and silica. Apatite 17 is enclosed within a troilite grain (Fig. 3I).

VHK basalt 14304,177 contains interstitial K-rich areas and vein-like structures that are situated between pyroxene and plagioclase crystals. In places the K-rich veins contain K-feldspar, K-rich glass (appearing brown in plane polarised light), merrillite, baddeleyite, and apatite (an example is shown in Fig. 4A). In this sample, the apatite crystals are restricted to the K-rich regions and typically range from ~50 to >300 µm in the longest dimension. Most of the apatite observed are subhedral and are usually heavily fractured (Fig. 4B).

Apatite in sample 15386 is almost exclusively found within mesostasis pockets surrounded by plagioclase and/or pyroxene crystals. Apatite 2 is found in contact with K-feldspar, ilmenite, and pyroxene, and it surrounds a pocket of K-feldspar. Apatite 2 is subhedral and occurs as blades up to ~100 µm in length (Fig. 4C). Apatite 5 is an anhedral grain ~250 µm in length that is in direct contact with merrillite, plagioclase and K-feldspar (Fig. 4D). Apatite 10 is a subhedral crystal that is ~25 µm in the longest dimension occurring inter-grown with merrillite. The crystal is enclosed in mesostasis glass and troilite.

Sample 76535,51 contains three crystals of apatite as reported in Barnes et al. (2014). Each crystal co-exists with merrillite and is located between plagioclase crystals. The largest apatite crystal is also found in contact with a symplectite assemblage (consisting of Mg–Al chromite and two pyroxenes, Elardo et al., 2012) and clinopyroxene (Fig. 5A, Barnes et al., 2014). Apatite crystals range from anhedral to subhedral and range in size from ~50 µm to ~250 µm. Apatite in thin-section 78235,43 are either found in small pockets of mesostasis containing Fe-metal, silica, merrillite, and clinopyroxene or associated with the main rock-forming orthopyroxene and plagioclase grains. Apatite occurs as subhedral grains up to ~95 µm in length and are generally heavily cracked (Fig. 5B).

Granulitic breccia 79215 is composed of both a matrix portion dominated by an anorthositic troctolite composition and a troc-

Table 1
Measured chlorine isotopic compositions (‰), and background corrected Cl contents (ppm) and H_2O contents (ppm) for the lunar apatite crystals studied in this work.

Sample type	Sample ID	Analysis ID	Cl content (ppm)	2σ (ppm)	δ^{37}Cl SMOC (‰)	2σ (‰)	H_2O content (ppm)	2σ (ppm)
High-Ti basalts	10044	Ap5b_10044_28Aug15	258	4	16.1	4.0	805	59
		Ap6Da_10044_28Aug15	209	3	6.8	4.5	754	55
		Ap6Ca_10044_28Aug15	375	5	10.0	3.3	716	52
		Ap6Cb_10044_28Aug15	1109	16	6.5	2.0	504	37
	10058	Ap5_10058_Cl_15Feb	493	14	4.9	3.7	1350	39
		Ap4a_10058_Cl_15Feb15	643	19	2.2	2.6	893	26
		Ap4b_10058_Cl_15Feb15	421	12	5.3	3.0	1845	53
		Ap6a_10058_Cl_16Feb15	2478	57	9.8	2.4	281	6
		Ap6b_10058_Cl_16Feb15	1139	26	5.0	2.7	1186	25
		Ap3_10058_Cl_16Feb15	594	14	5.6	3.1	888	19
		Ap3b_10058_Cl_16Feb15	632	14	9.9	3.0	1236	26
	70035	Ap17_70035_27Aug15 n1	968	14	14.4	2.1	578	42
		Ap17_70035_27Aug15 n2	1379	20	13.4	1.8	547	40
		Ap15_70035_27Aug15 n1	746	11	10.8	2.5	412	30
Low-Ti basalt	15555	Ap1a_15555_Cl_18Feb	3143	47	12.8	1.5	1786	19
		Ap1b_15555_Cl_18Feb	3306	50	13.8	1.5	2268	24
		Ap5b_15555_Cl_18Feb	847	13	12.7	2.1	1298	14
VHK basalt	14304	Ap1a_14304_Cl_16Feb15	2862	66	28.1	1.5	64	1
		Ap1b_14304_Cl_16Feb15	4084	94	29.4	1.4	114	2
		Ap2a_14304_Cl_17Feb15	4100	94	24.5	2.8	123	3
		Ap4a_14304_Cl_17Feb15	2453	56	27.9	2.5	52	1
		Ap4b_14304_Cl_17Feb15	4148	95	25.9	2.5	82	2
		Ap4c_14304_Cl_18Feb	5878	88	27.8	2.4	50	1
		Ap4d_14304_Cl_18Feb	4940	74	29.0	2.4	74	1
		Ap5a_14304_Cl_18Feb	3779	57	31.7	2.5	59	1
		Ap5b_14304_Cl_18Feb	3815	57	28.8	2.5	103	1
		Ap8_14304_Cl_18Feb	4331	65	28.5	2.5	57	1
KREEP basalt	15386	Ap5a_15386_29Aug15	3764	55	30.8	1.3	136	10
		Ap10a_15386_29Aug15	2720	40	22.5	1.5	484	35
		Ap2a_15386_29Aug15	987	14	14.1	2.2	198	14
Mg-suite	76535	Ap3aCl_76535_13Feb	13163	164	31.1	1.2	*b.d.*	–
		Ap3bCl_76535_13Feb	13428	167	32.1	1.3	*b.d.*	–
	78235	Ap7a_78235_19Feb	13689	205	31.2	1.6	79	1
		Ap7b_78235_19Feb	13301	199	28.9	1.6	40	1
		Ap5a_78235_19Feb	12322	185	29.6	1.6	195	2
		Ap5b_78235_19Feb	10110	152	28.9	1.7	168	2
		Ap3a_78235_19Feb15	11435	171	29.1	1.2	25	0
		Ap3b_78235_19Feb15	10757	161	32.8	1.2	35	1
		Ap5c_78235_19Feb15	10897	163	33.8	1.2	67	1
Granulite	79215	79215_Ap13a	7165	523	29.3	0.9	33	15
		79215_Ap13b	7331	535	26.6	0.9	36	16
		79215_Ap13c	7036	514	26.9	0.9	32	14
		79215_Ap13d	7209	526	28.1	0.9	38	17
		79215_Ap13e	7293	533	27.6	0.9	34	15
		79215_Ap1_27Nov	6349	464	25.1	1.8	47	21
		79215_Ap1_27Novb	7561	552	31.7	1.6	156	70
		Ap3aCl_79215_12Feb15	7241	123	34.8	2.0	106	2
		Ap3b_79215Cl_12Feb15	7345	124	36.3	2.0	*b.d.*	–
		Ap2aCl_79215_13Feb15	7605	94	30.0	2.0	*b.d.*	–
		Ap12aCl_79215_13Feb15	7169	89	33.8	2.0	*b.d.*	–

b.d. indicates analyses that are below detection limits.

tolitic portion. Apatite is abundant in this thin-section of sample 79215, occurring exclusively in the troctolite portion and in direct contact with olivine, plagioclase, and troilite. Texturally, the apatite contains rounded blebs of pre-existing plagioclase and olivine, with lobate crystal edges. All of the apatite crystals are anhedral to subhedral and range from ~30 to >300 μm in the longest dimension (Fig. 5C).

3.2. Intra-sample variations of the isotopic and chemical composition of apatite

A total of twenty nine apatite grains from the eight samples were analysed for their Cl abundances and Cl-isotopic signatures and the results are provided in Table 1 and shown in Fig. 6. The Cl-isotopic composition of apatite in 10044 is variable and seems to be related to the textural context of the grains. Apatite crystal Ap5, which is characterised by δ^{37}Cl value of $+16.1 \pm 4.0$‰, can be assumed to have formed early because it is in contact with plagioclase and pyroxene but not with the late-stage mesostasis assemblage. In contrast, apatite grains 6C and 6D are located in separate mesostasis areas (Fig. 3) and yet record similar Cl-isotopic compositions of $+6.5 \pm 2.0$ to $+10.0 \pm 3.3$‰. Cl content is variable between, and within, the grains ranging from 0.02 to 0.11 wt% Cl. Among the mare basalts, sample 10058 yielded apatite Cl contents from 0.04 to 0.25 wt% and δ^{37}Cl values from $+2.2 \pm 2.6$ to $+9.9 \pm 3.0$‰. Given the analytical uncertainties, it is not possible to distinguish between the average δ^{37}Cl values ($+3.8 \pm 4.5$‰) for apatite crystals 4 and 5, both located in contact with K-feldspar, and apatite 3 and 6, which are in contact with other late-crystallised minerals (average δ^{37}Cl values,

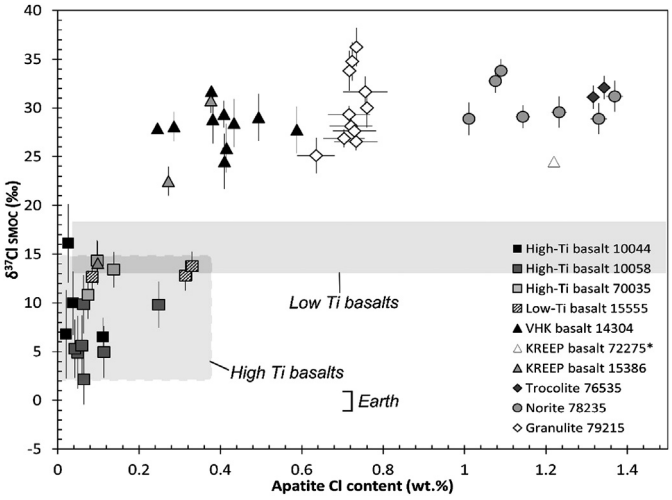

Fig. 6. New Cl-isotope data (‰) plotted against Cl content for lunar apatite in the samples studied. Measured Cl-isotope ratios are referenced to Standard Mean Ocean Chloride (SMOC). Uncertainties represent 2σ errors (see text for details). Data for basalt fields: low-Ti and high-Ti basalt (Sharp et al., 2010; Boyce et al., 2015), *KREEP basalt 72275 (Sharp et al., 2010), and the Earth range (Sharp et al., 2013a).

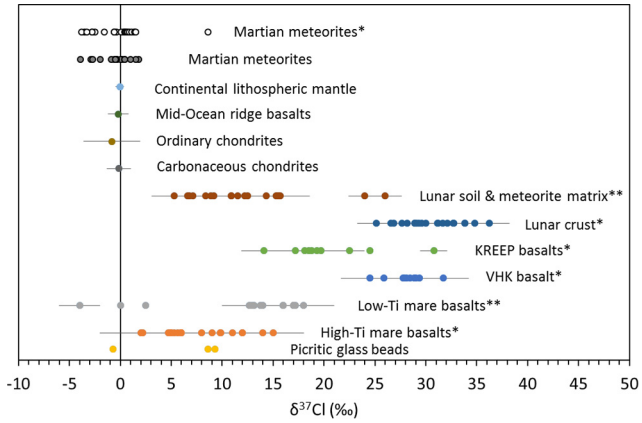

Fig. 7. Plot comparing the chlorine isotopic compositions of different objects in the Solar System. All of the data available for lunar samples (Sharp et al., 2010; Treiman et al., 2014; Tartèse et al., 2014b; Boyce et al., 2015; this study) have been plotted together with their individual uncertainties. * data from the *in situ* analyses of apatite and ** data included from both *in situ* analyses of apatite and bulk Cl isotope measurements. Also plotted are the new data Cl isotope measurements of martian meteorites from Williams et al. (in press), both bulk measurements (grey symbols) and *in situ* apatite measurements (denoted by *). The average δ^{37}Cl values for the Earth's continental mantle, mid-ocean ridge basalts, Earth, ordinary and carbonaceous chondrites have been plotted with the uncertainties representing the 2σ standard deviation of the literature values (Sharp et al., 2013a).

$+7.7 \pm 4.2$‰). Apatite crystals in mare basalt 70035 have relatively restricted Cl-isotopic compositions with δ^{37}Cl values ranging from $+10.8 \pm 2.5$‰ to $+14.4 \pm 2.1$‰. There is inter- and intra-grain variability in Cl content, with apatite 15 containing ~0.07 wt% Cl whereas Cl content varies between ~0.10 and 0.14 wt% Cl for apatite 17. Low-Ti basalt 15555 contains apatite characterised by Cl abundances between 0.08 and 0.33 wt% Cl and almost invariant δ^{37}Cl values of approximately $+13 \pm 2$‰ in all of the exhibited petrographic contexts.

In contrast, VHK basalt 14304,177 contains more Cl-rich apatite, with Cl contents between 0.29 and 0.59 wt% associated with heavy δ^{37}Cl compositions falling in the range between $+24.5 \pm 2.8$ and $+31.7 \pm 2.5$‰. In the case of KREEP basalt 15386, all three apatite crystals analysed are located in mesostasis, so it is challenging to determine the relative timing of crystallisation, which was previously done for D/H ratios and H_2O content in another thin-section of 15386 (Tartèse et al., 2014a). Apatite in the thin section of 15386 studied here are characterised by a large range of δ^{37}Cl values from $+14.1 \pm 2.2$‰ to $+30.8 \pm 1.3$‰ and display a similarly large spread in Cl contents from ~0.1 to 0.4 wt%. There is a positive correlation between apatite Cl contents and associated isotopic composition in KREEP basalt 15386.

With regards to the apatite crystals in lunar highlands samples, lunar troctolite 76535 contains Cl-rich apatite containing $\sim 1.32 \pm 0.02$ wt% Cl and uniform δ^{37}Cl values of between $+31.1 \pm 1.2$ and $+32.1 \pm 1.2$‰ (Table 1). Similarly, apatite grains in cumulate norite 78235 contain between 1.01 and 1.37 wt% Cl associated with δ^{37}Cl values ranging between $+28.9 \pm 1.7$ and $+33.8 \pm 1.2$‰. Finally, apatite in the impact-related granulite 79215 are characterised by homogeneous Cl contents (weighted average 0.74 ± 0.02 wt% Cl, $n = 11$) but display a large range of Cl isotopic compositions, with δ^{37}Cl values ranging from $+25.1 \pm 1.8$ up to $+36.3 \pm 2.0$‰.

4. Discussion

4.1. Comparing the Cl-isotopic compositions of lunar apatite

Generally, apatite in the mare basalts studied here and previously (Sharp et al., 2010; Tartèse et al., 2014b; Boyce et al., 2015) shows a broad range of δ^{37}Cl values that extend from ~−4 to +18‰, lower than those measured in apatite in lunar highlands samples and the VHK basalt (~+25 to +36‰, Fig. 6). To date, the only lunar basalts to exhibit very heavy apatite chlorine isotope compositions (>+18‰) are KREEP-related basalts (Sharp et al., 2010; Tartèse et al., 2014b; McCubbin et al., 2015a). The KREEP basalts are those whose parental melts assimilated a significant KREEP component, hence they have geochemical characteristics of both their mantle source and urKREEP. Collectively, apatite in the KREEP (15386 (this study) and 72275 (Sharp et al., 2010)) and VHK (14304) basalts are characterised by δ^{37}Cl values between $+14.1 \pm 2.2$ and $+31.7 \pm 2.5$‰ and display a large spread of chlorine contents from approximately 0.1 to 1.2 wt% (Fig. 6). Apatite from lunar highlands samples (76535 and 78235) are characterised by more homogeneous Cl-isotopic compositions (δ^{37}Cl in the range of ~+29 to +34‰) and have the highest Cl abundances when compared to apatite from mare basalts. Apatite in lunar granulite 79215 display some of the highest chlorine isotopic compositions recorded for Solar System materials (Fig. 7), up to $+36.3 \pm 2.0$‰ (Table 1).

4.2. Reconciling H- and Cl-isotope measurements of lunar apatite

The hydrogen isotopic compositions of OH in apatite from the high-Ti and low-Ti mare basalts are highly variable, but some of the observed values can be reconciled if the parent magmas had undergone H_2-degassing upon ascent and eruption. This process would have caused non-degassed H_2O left behind in the magmas to have elevated δD values, which is recorded by apatite that crystallised during or after degassing (Tartèse et al., 2013). The modelled un-degassed (or pre-degassing) δD value for the parental magmas of the mare basalts is approximately $\sim 0 \pm 200$‰ (e.g., Tartèse et al., 2014a), which is consistent with that modelled for the un-degassed parent magmas of lunar ultramafic glass beads (Saal et al., 2013; Füri et al., 2014). However, a direct link between degassing of H_2 and elevated H-isotopic composition remain elusive because of the paucity of spatially resolved H-isotopic analyses in support of the degassing model. A study of lunar KREEP basalts by Tartèse et al. (2014a) was able to bridge the gap between measured data and modelling of H_2-degassing based on spatially correlated H-isotopic analyses of apatite in KREEP basalt 15386. Specifically, they observed that earlier-formed apatite included within pyroxene exhibited lower δD values ($+98 \pm 99$‰)

and elevated H_2O abundances in comparison to later-formed apatite within late-stage mesostasis areas (highest δD values of +615 to +778‰). This observation marked the first direct link between degassing of H_2 and elevated δD values in lunar basalts. Füri et al. (2014) also observed an inverse correlation between δD values and H_2O abundances in high-Ti picritic glass beads, which they interpreted as the consequence of extensive Rayleigh-type degassing of H_2 from melts initially containing H_2O characterised by a δD value ~−100‰. Interestingly, the lowest δD value recorded in apatite from 15386 is +98 ± 99‰, which is consistent with the estimates of the parental melt δD values modelled previously from apatite in low- and high-Ti mare basalts (Tartèse et al., 2013), as well as the pyroclastic glass beads (e.g., Saal et al., 2013; Füri et al., 2014).

Magmatic degassing has also been invoked to explain the departure of lunar Cl-isotopic compositions from the terrestrial mantle value (~−0.2 ± 1.0‰ Fig. 7; Sharp et al., 2013a). Sharp et al. (2010) suggested that the volatilisation of metal chlorides during magma ascent and eruption could fractionate the lighter ^{35}Cl isotope from heavier ^{37}Cl, a process requiring very low H/Cl ratios at the time of chloride degassing in order to promote the loss of metal chlorides relative to HCl, because degassing of HCl from a magma would not fractionate Cl isotopes. In such a model, degassing would favour the loss of light metal chloride isotopologues (i.e., those containing ^{35}Cl instead of ^{37}Cl), for example $FeCl_2$ or $ZnCl_2$, leaving residual chlorine dissolved in the magma enriched in ^{37}Cl (Sharp et al., 2010; Ustunisik et al., 2011, 2015). This ^{37}Cl-enriched signature would then be recorded in the rocks through the incorporation of Cl into Cl-bearing mineral phases like apatite that crystallise from the residual melt.

In fact, it has recently been demonstrated experimentally that during ascent of volatile-rich magmas, hydrogen is likely to be the earliest volatile to degas, and after H is depleted in the melt, Cl becomes the preferred volatile that is lost (Sharp et al., 2013b; Ustunisik et al., 2015), supporting the requirement for very low H/Cl ratios in magmas at the time of Cl degassing. However, it remains unclear whether successive episodes of volatile-degassing from a single magma could explain both elevated δD and elevated δ^{37}Cl values measured in apatite in mare basalts. Indeed, the requirements of very low H/Cl ratios in the melt to account for the elevated δ^{37}Cl values measured, which was proposed by Sharp et al. (2010), seems incompatible with the occurrence of OH-rich apatite relative to Cl in the mare basalts (Tartèse et al., 2013; McCubbin et al., 2015a) given the relative preference of Cl over H into crystallising apatite (Boyce et al., 2014; McCubbin et al., 2015b), which should result in very OH-poor apatite (Ustunisik et al., 2015). In addition, the effects of HCl degassing from basaltic melts on the fractionation of Cl isotopes has never been investigated under conditions relevant to mare basalt petrogenesis (e.g., low oxygen fugacity under vacuum), adding to the complexity of interpreting combined apatite δD and δ^{37}Cl values. In any case, it is likely that variations of apatite δD and δ^{37}Cl values have resulted from the interplay between different magmatic processes such as degassing or mixing, potentially overprinting of any geochemical signatures inherited from previously-formed isotopic reservoirs. As stated above, there is a positive correlation between apatite Cl contents and associated isotopic composition in KREEP basalt 15386. If degassing of a Cl-bearing vapour was influencing the Cl-isotopic composition, then the opposite correlation would be expected (Ustunisik et al., 2011, 2015). However a positive correlation between Cl abundance and δ^{37}Cl values of apatite is consistent with the assimilation of a δ^{37}Cl-enriched component, which has also been reported recently in martian rocks (Williams et al., in press).

To identify the primordial chlorine and hydrogen isotopic compositions of the lunar interior and identify any specific isotopic reservoirs, pristine samples that are unlikely to have undergone magmatic degassing of volatiles during ascent and crystallisation should be targeted. From the literature, there are at least two KREEP-rich samples, KREEP basalt 72275 (Tartèse et al., 2014a) and Mg-suite norite 78235 (Barnes et al., 2014), which are considered to directly record the H-isotopic composition of their un-degassed parent melts, so we will first address the isotopic composition of H in the Moon. Apatite in 72275 contain appreciable amounts of OH that appears not to have undergone magmatic degassing, since apatite in this sample seems to have retained the original un-degassed δD value of the parent melt (i.e., average −113‰ ± 62‰; Tartèse et al., 2014a). Sample 78235 is a plutonic norite sample containing apatite that exhibits relatively homogeneous H-isotopic compositions (i.e., average −27‰ ± 98‰; Barnes et al., 2014). These samples have had different petrological histories (see Supplementary Information), but the parental magmas of both samples are considered to have assimilated urKREEP, or interacted with a derivative of urKREEP (Barnes et al., 2014; Tartèse et al., 2014a; Shearer et al., 2015). Therefore, the H-isotopic signatures of OH in apatite from these samples, −27 ± 98‰ for 78235 (Barnes et al., 2014) and −113 ± 62‰ for 72275 (Tartèse et al., 2014a), identical within error, can be interpreted as reflecting the H-isotopic composition of H_2O in urKREEP. Notably, the H-isotopic composition of urKREEP determined from these un-degassed samples matches the measured and modelled values for the mare source in the lunar mantle (Saal et al., 2013; Füri et al., 2014; Tartèse et al., 2014a). Consequently, it appears that the H-isotopic composition of the bulk Moon could be relatively homogeneous (within a few hundred ‰) and similar to the terrestrial mantle (e.g., Lécuyer et al., 1998; Hallis et al., 2015), consistent with assertions that the Earth–Moon system acquired water from a similar source (Alexander et al., 2012; Saal et al., 2013; Barnes et al., 2014; Sarafian et al., 2014).

We now consider the Cl-isotopic compositions of apatite from these same un-degassed samples, 72275 and 78235. Apatite in both samples are characterised by heavy chlorine isotopic compositions (this study and Sharp et al., 2010), which is perplexing, given the existing evidence that these samples did not undergo substantial magmatic degassing (i.e., measurable OH abundances inconsistent with very high melt Cl/H ratios and homogeneous intra-sample δD values). Alternatively, the parental melts of these samples were derived from, or mixed with, a heavy Cl component, and the elevated δ^{37}Cl values are unrelated to degassing at or before the time of apatite crystallisation. As noted previously, both samples have a substantial KREEP-component, which has been identified previously as a potential reservoir characterised by elevated δ^{37}Cl (McCubbin et al., 2015a; Boyce et al., 2015). Additionally, Mg-suite troctolite 76535, another KREEP-rich sample, and one of the few un-shocked pristine lunar cumulate samples available for study, is also characterised by elevated δ^{37}Cl values of ~+30‰ (Table 1). Based on existing petrogenetic models for the highlands samples, their inventory of volatiles, including Cl, comes predominantly from urKREEP (Barnes et al., 2014; McCubbin et al., 2015a; Shearer et al., 2015), and so these samples are likely representative of the Cl-isotopic composition of urKREEP (McCubbin et al., 2015a). Together these observations provide strong evidence that the Cl-isotopic composition of urKREEP is elevated and is likely to be ~ +30‰. In contrast, samples from the mare basalt source region(s) within the lunar mantle exhibit a wide range of Cl isotopic compositions that extend down to −4‰ (Sharp et al., 2010; Boyce et al., 2015), indicating that different reservoirs in the Moon's interior may have different Cl-isotopic composition.

4.3. Relating heavy Cl-isotopic compositions to a KREEP component

We further investigated whether the heavy Cl-isotope signature could be related to the proportion of KREEP component in

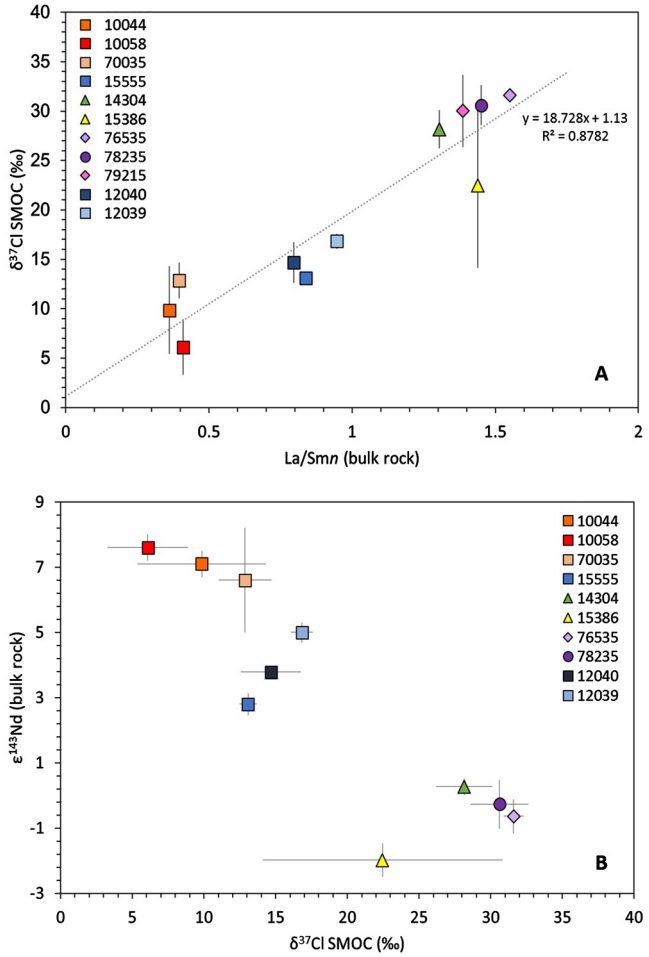

Fig. 8. New Cl-isotopic data for lunar apatite compared to (A) carbonaceous chondrite-normalised La/Sm bulk-rock ratios (normalised ('*n*') using La/Sm ratios of carbonaceous chondrites given by Anders and Grevesse (1989), see Supplementary Table 2) and (B) ε^{143}Nd initial values and uncertainties (Supplementary Table 2) versus the average Cl-isotopic composition of apatite. All Cl-isotope values are the average δ^{37}Cl values for each sample and the uncertainties represent the standard deviation. The Cl isotope data for 12040 and 12039 are from Boyce et al. (2015).

lunar samples by correlating Cl isotope compositions with bulk-rock incompatible trace element (La, Sm and ε^{143}Nd initial) data (Supplementary Table 2). Fig. 8A shows a strong positive correlation between apatite δ^{37}Cl values and La/Sm ratios (La/Sm_n), which strongly indicates mixing between a mantle source with low δ^{37}Cl isotopic composition (~0‰, Y-intercept in Fig. 8A) and a KREEP-rich component characterised by a δ^{37}Cl value ~+30‰. Similarly, basaltic rocks originating from KREEP-poor LMO source regions characterised by lighter δ^{37}Cl values are associated with positive bulk-rock ε^{143}Nd initial values >2–3 (Fig. 8B and Supplementary Table 2).

In summary, there is a clear grouping between KREEP-rich rocks, such as those from the Mg-suite, KREEP basalts, and VHK basalts, characterised by elevated δ^{37}Cl values, and less KREEPy rocks, such as the high- and low-Ti mare basalts, characterised by lower δ^{37}Cl values. These observations confirm that the KREEP component, and by extension urKREEP, was characterised by extremely heavy δ^{37}Cl values while the mantle source regions of mare basalts had a terrestrial-like Cl-isotopic composition.

4.4. LMO degassing and vapour speciation: Implications for H-isotopes

Hydrogen and chlorine are both incompatible elements that are soluble in silicate melts (Cl more so than H), so it is reasonable to assume that both would be concentrated in urKREEP (e.g., review by McCubbin et al., 2015a). Furthermore, the H/Cl ratio of urKREEP is reported to be <1 (McCubbin et al., 2015a). Based on the work of Fegley (1991), in which thermodynamic activities of volatiles under lunar conditions were considered, he concluded that the dominant species likely to be degassed when H/Cl <1 were HCl and HF in the case of H species and metal chlorides (and fluoride species) as the dominant species carrying the halogens. For lunar magmas, H_2 is also likely to be an important degassing species (Richet et al., 1977; Ustunisik et al., 2015). Any degassing of H in the form of HCl or H_2 would result in similar H and D fractionations (Richet et al., 1977), as calculated by Tartèse et al. (2013) (Supplementary Fig. 2).

It is important to consider the possibility that H degassing could have occurred simultaneously with Cl loss. The current estimates for the H-isotopic composition of H_2O in urKREEP range from as low as −400 to +200‰ (Barnes et al., 2014; Tartèse et al., 2014a). In the framework of Cl degassing (metal chlorides as the major Cl carrier) from urKREEP, it is likely that H was also degassed in the form of HCl and/or H_2. If the lowest measured δD value of highlands apatite is considered as the pre-degassing urKREEP signature (77215, ~−400‰, Barnes et al., 2014), then the observations from KREEPy lithologies can be reconciled with differential (0 to 99%) degassing of H_2 and/or HCl (Supplementary Fig. 2). Such low initial δD values are consistent with recently proposed values for the Earth's upper mantle (Sharp et al., 2013b; Hallis et al., 2015) or for some evolved lithologies from the Moon (Robinson et al., 2014). If the pre-degassing H-isotopic composition of H in urKREEP was heavier than ~−400‰, for example −200 or 0‰, then 99% degassing of H_2 would increase the δD value to >+400–500‰. However, such signatures have yet to be observed in apatite from KREEP-rich lithologies considered to be unaffected by degassing (e.g., KREEP basalt 72275 and Mg-suite norite 78235), which implies that either in this scenario only partial (<95%) degassing of H occurred, or that the heavy degassed signature was overprinted by volatiles added by carbonaceous chondrites during late accretion (e.g., Alexander et al., 2012; Bottke et al., 2010). The LMO period in the Moon's evolution is highly unlikely to have been quiescent and it has been proposed by many (e.g., Day et al., 2007; Bottke et al., 2010; Kamata et al., 2015) that impactors were accreting to the Moon during the LMO phase (Fig. 9). Therefore, it is not unreasonable to assume that some of these impactors contributed H_2O to the lunar interior during differentiation or after urKREEP degassing (e.g., Bottke et al., 2010) (Fig. 9 and calculations in the Supplementary Material). Importantly, if exogenous addition of volatiles to the Moon from objects with H/Cl ratios >1 (i.e., comets and carbonaceous asteroids) occurred, then it did not cause the resultant H/Cl ratio of the LMO residual liquid to exceed 1. If it had then this would have inhibited the fractionation of Cl in the LMO (discussed further in the next section).

In summary, our model does not preclude (a) the presence of H prior to metal chloride degassing from urKREEP nor (b) the possibility of at least some degassing of H in the form of HCl and/or H_2 during metal chloride loss from urKREEP.

4.5. LMO degassing and timing of ^{37}Cl enrichment of urKREEP

The internal differentiation of the Moon via a LMO predicts a volatile-rich urKREEP layer dominated by Cl, containing at least 1350 ppm Cl (McCubbin et al., 2015a). Boyce et al. (2015) have proposed that degassing of Cl from the LMO would account for fractionation of Cl isotopes and δ^{37}Cl values ~+30‰ in the residual urKREEP layer. In this model, the residual LMO becomes progressively enriched in ^{37}Cl relative to ^{35}Cl as metal chlorides are degassed (Boyce et al., 2015). Although this model fits the geochemical trends observed by Boyce et al. (2015) and in the present

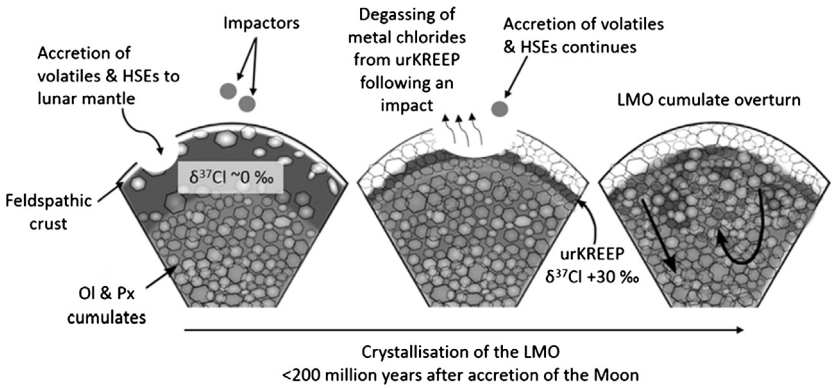

Fig. 9. Cartoon depicting the differentiation of the Moon via the lunar magma ocean (LMO) model. Chlorine is concentrated in the urKREEP layer after >80% crystallisation of the LMO. We suggest that one or several impacts, sufficiently large to penetrate the crust, provide the means of exposing the urKREEP layer (or KREEP rich melts) to vacuum and thus facilitates the fractionation of Cl through degassing of metal chlorides (Sharp et al., 2010). We anticipate that continued accretion (post-core formation) of asteroids (carbonaceous chondrite-like) likely took place during the ~10 to 200 million year lifetime of the LMO and that these impactors delivered quantities of highly siderophile elements (HSEs) and H_2O necessary to explain the source region compositions of the mare basalts (Tartèse et al., 2013), KREEP-rich samples (Barnes et al., 2014; Tartèse et al., 2014a, 2014b) and picritic glasses (Saal et al., 2013; Füri et al., 2014).

study (Fig. 8), there are a number of shortcomings to this early LMO degassing model. (1) The solubility of chloride in silicate melts is relatively high, even at low pressure (Webster and De Vivo, 2002). In fact, chloride solubility in basaltic liquids could have been on the order of ≥2.9 wt% (Cl^- solubility from Webster et al., 1999; Webster and De Vivo, 2002) at depths just below the lunar surface; consequently, Cl^- solubility was not likely to have been a driving factor for Cl loss. (2) Chloride is degassed from magmas even at low concentrations in an open system where the equilibrium partial pressure of chloride vapour cannot be attained (i.e., Ustunisik et al., 2011, 2015). This scenario is consistent with the one envisioned by Boyce et al. (2015); however, prior to the formation of a conductive lid in the LMO, there would have been an atmosphere in contact with the LMO surface (e.g., Saxena et al., 2016). It is difficult to determine the precise composition or pressure of that atmosphere, but it would have certainly hindered the early loss of metal chlorides, which is maximised when the magma is in contact with a vacuum. (3) Before the formation of a conductive lid (i.e., early LMO degassing), metal chloride vapours that degassed would condense into chloride salts upon cooling and rain back into the atmosphere or the LMO (i.e., they would be unlikely to escape lunar gravity), and it is not clear that a heavy Cl isotopic reservoir would result from this process. Consequently, we agree with Boyce et al. (2015) that loss of Cl from the LMO could have occurred throughout the lifetime of the LMO, but we are not convinced that it would have necessarily resulted in a δ^{37}Cl-enriched urKREEP layer at the base of the anorthosite crust.

A model in which urKREEP was exposed to high vacuum subsequent to the formation of the anorthosite crust, after the dissipation of the LMO atmosphere, circumvents all three of the potential issues raised above with the Boyce et al. (2015) model of early LMO degassing of metal chlorides. Consequently, we envisage a scenario in which during the latter stages of LMO crystallisation (>95%), a large bolide, or series of bolides, punctured the lunar crust (Kamata et al., 2015) to a depth sufficient to expose the Cl-rich urKREEP layer, or bring KREEP-rich melts up to the strong vacuum at the lunar surface, which initiated degassing of metal chlorides (Sharp et al., 2010). The degassed metal chlorides would be drawn into cold traps (i.e., regions of the surface surrounding the melt pool that would be substantially cooler than the melt) in the surrounding crust and regolith where the metal chloride vapour would condense back into chloride salts, leading to the formation of ^{37}Cl-rich urKREEP residual melts (Fig. 9).

Degassing of >80% of the initial Cl content by such a process would have resulted in an urKREEP layer with a heavy δ^{37}Cl value of around +30‰ (Supplementary Fig. 1). Interestingly, the Bulk Silicate Moon (BSM) estimate of ~10 ppm Cl (McCubbin et al., 2015a) corresponds to a pre-degassing BSM Cl content of ~100–500 ppm (for 90 to 98% Cl degassed), which is well within the range of Cl abundances in carbonaceous chondrites (e.g., Sharp et al., 2013a). It is possible that the isotopic composition of other moderately volatile elements, such as Zn (e.g., Kato et al., 2015), S (Wing and Farquhar, in press) and even refractory elements such as Fe (Wang et al., 2015), in the urKREEP liquid could have been fractionated by the same event(s) that degassed Cl (Fig. 9).

The scenario we propose to account for the elevated Cl isotope composition of urKREEP involves a large (or multiple) impact event(s) during the first 150 to 200 million years (Kamata et al., 2015) of the Moon's history, which is consistent with the requirement for post-core formation addition of highly siderophile elements (HSEs) (Day et al., 2007) and other volatiles such as H (Albarède et al., 2013; Tartèse et al., 2013; Füri et al., 2014; Hauri et al., 2015) and N (Füri et al., 2015) to the lunar mantle. Given the spatial association of the Apollo sampling sites and the Procellarum KREEP Terrane (PKT), the surface expression of KREEP is presumably represented by the PKT region (Jolliff et al., 2000). Although the PKT does not show evidence from gravity data as being an impact basin (Andrews-Hanna et al., 2014), impacts as early as those required to expose the residual LMO liquid may not be preserved due to viscoelastic relaxation of the early hot lunar crust (e.g., Kamata et al., 2015). Consequently, one would expect that samples from outside of the PKT and nearside Apollo-sampled region of the Moon to have chondritic and terrestrial-like Cl-isotopic compositions. This hypothesis could be tested through future sample return missions that target regions on the lunar surface far outside the PKT region.

5. Summary

The aims of this study were to (i) thoroughly investigate the apparently unique Cl isotope compositions of lunar samples, (ii) to reconcile new and existing H and Cl data for lunar samples in order to identify potential volatile reservoirs within the Moon, and (iii) to assess the requirement for early Cl degassing from the lunar magma ocean as predicted by previous work. To achieve this, we have measured the Cl-isotopic compositions of apatite in a diverse range of lunar samples, ranging in lithologies from mare basalts, to KREEP and VHK basalts and pristine highlands samples. The samples studied show Cl-isotopic compositions ranging from ~+2 to ~+36‰, and reveal a stark difference between KREEP-poor and KREEP-rich samples. We have provided strong evidence

that lunar samples obtained their exotic heavy Cl-isotopic compositions by variable incorporation of urKREEP (δ^{37}Cl of $\sim$+30‰). We hypothesise that the differentiation of the Moon via a LMO provides the most elegant mechanism for concentrating volatiles, especially Cl, into a residual melt (urKREEP). In order to account for the Cl-isotopic composition of urKREEP, this residual melt had to degas following enrichment at relatively low pressures, and for this we invoke puncturing of the lunar crust by one or several large impact events, prior to the solidification of the urKREEP liquid in the LMO.

Acknowledgements

We thank NASA CAPTEM for allocation of lunar samples (to MA and CRN). This research was supported by a grant from the UK Science and Technology Facilities Council (grant # ST/L000776/1 to M.A. and I.A.F.). FMM acknowledges support from NASA's LASER program during this study through grant NNX13AK32G. We thank Erik Hauri and Evelyn Füri for their insightful reviews which helped to improve this manuscript, and we thank the editor Bernard Marty for his handling of this manuscript.

Appendix A. Supplementary material

Supplementary material related to this article can be found online at http://dx.doi.org/10.1016/j.epsl.2016.04.036.

References

Albarède, F., et al., 2013. Asteroidal impacts and the origin of terrestrial and lunar volatiles. Icarus 222, 44–52.
Alexander, C.M.O., et al., 2012. The provenances of asteroids, and their contributions to the volatile inventories of the terrestrial planets. Science 337, 721–723.
Anders, E., Grevesse, N., 1989. Abundances of the elements: meteoritic and solar. Geochim. Cosmochim. Acta 53, 197–214.
Andrews-Hanna, J.C., et al., 2014. Structure and evolution of the lunar Procellarum region as revealed by GRAIL gravity data. Nature 514, 68–71.
Barnes, J.J., et al., 2014. The origin of water in the primitive Moon as revealed by the lunar highlands samples. Earth Planet. Sci. Lett. 390, 244–252.
Barnes, J.J., et al., 2013. Accurate and precise measurements of the D/H ratio and hydroxyl content in lunar apatites using NanoSIMS. Chem. Geol. 337, 48–55.
Boyce, J.W., et al., 2015. The chlorine isotope fingerprint of the lunar magma ocean. Sci. Adv. 1, e1500380.
Boyce, J.W., Tomlinson, S.M., McCubbin, F.M., Greenwood, J.P., Treiman, A.H., 2014. The lunar apatite paradox. Science 344, 400–402.
Boyce, J.W., et al., 2010. Lunar apatite with terrestrial volatile abundances. Nature 466, 466–469.
Bottke, W.F., Walker, R.J., Day, J.M.D., Nesvorny, D., Elkins-Tanton, L., 2010. Stochastic late accretion to Earth, the Moon, and Mars. Science 330, 1527–1530.
Canup, R.M., Visscher, C., Salmon, J., Fegley Jr., B., 2015. Lunar volatile depletion due to incomplete accretion within an impact-generated disk. Nat. Geosci. 8, 918–921.
Canup, R.M., 2012. Forming a Moon with an Earth-like composition via a giant impact. Science 338, 1052–1055.
Ćuk, M., Stewart, S.T., 2012. Making the Moon from a fast-spinning Earth: a giant impact followed by resonant despinning. Science 338, 1047–1052.
Day, J.M.D., Pearson, G.D., Taylor, L.A., 2007. Highly siderophile element constraints on accretion and differentiation of the Earth–Moon system. Science 315, 217–219.
Elardo, S.M., McCubbin, F.M., Shearer, C.K., 2012. Chromite symplectites in Mg-suite troctolite 76535 as evidence for infiltration metasomatism of a lunar layered intrusion. Geochim. Cosmochim. Acta 87, 154–177.
Elardo, S.M., Draper, D.S., Shearer, C.K., 2011. Lunar magma ocean crystallization revisited: bulk composition, early cumulate mineralogy, and the source regions of the highlands Mg-suite. Geochim. Cosmochim. Acta 75, 3024–3045.
Elkins-Tanton, L.T., Grove, T.L., 2011. Water (hydrogen) in the lunar mantle: results from petrology and magma ocean modelling. Earth Planet. Sci. Lett. 307, 173–179.
Elkins-Tanton, L.T., Burgess, S., Yin, Q-Z., 2011. The lunar magma ocean: reconciling the solidification process with lunar petrology and geochronology. Earth Planet. Sci. Lett. 304, 326–336.
Elkins-Tanton, L.T., Van Orman, J.A., Hager, B.H., Grove, T.L., 2002. Re-examination of the lunar magma ocean cumulate overturn hypothesis: melting or mixing is required. Earth Planet. Sci. Lett. 196, 239–249.
Fegley, B., 1991. Thermodynamic models of the chemistry of lunar volcanic gases. Geophys. Res. Lett. 18, 2073–2076.
Füri, E., Barry, P.H., Taylor, L.A., Marty, B., 2015. Indigenous nitrogen in the Moon: constraints from coupled nitrogen–noble gas analyses of mare basalts. Earth Planet. Sci. Lett. 431, 195–205.
Füri, E., Deloule, E., Gurenko, A., Marty, B., 2014. New evidence for chondritic lunar water from combined D/H and noble gas analyses of single Apollo 17 volcanic glasses. Icarus 229, 109–120.
Greenwood, J.P., et al., 2011. Hydrogen isotope ratios in lunar rocks indicate delivery of cometary water to the Moon. Nat. Geosci. 4, 79–82.
Hallis, L.J., et al., 2015. Evidence for primordial water in Earth's deep mantle. Science 350, 795–797.
Hauri, E.H., Saal, A.E., Rutherford, M.J., Van Orman, J.A., 2015. Water in the Moon's interior: truth and consequences. Earth Planet. Sci. Lett. 409, 252–264.
Jolliff, B.L., Gillis, J.J., Haskin, L.A., Korotev, R.L., Wieczorek, M.A., 2000. Major lunar crustal terranes: surface expressions and crust–mantle origins. J. Geophys. Res., Planets 105, 4197–4216.
Kamata, S., et al., 2015. The relative timing of Lunar Magma Ocean solidification and the late heavy bombardment inferred from highly degraded impact basin structures. Icarus 250, 492–503.
Kato, C., Moynier, F., Valdes, M.C., Dhaliwal, J.K., Day, J.M.D., 2015. Extensive volatiles loss during the formation and differentiation of the Moon. Nat. Commun. http://dx.doi.org/10.1038/ncomms8617.
Lécuyer, C., Gillet, P., Robert, F., 1998. The hydrogen isotope composition of seawater and the global water cycle. Chem. Geol. 145, 249–261.
McCubbin, F.M., et al., 2015a. Magmatic volatiles (H, C, N, F, S, Cl) in the lunar mantle, crust, and regolith: abundances, distributions, processes, and reservoirs. Am. Mineral. 100, 1668–1707.
McCubbin, F.M., et al., 2015b. Experimental investigation of F, Cl, and OH partitioning between apatite and Fe-rich basaltic melt at 1.0–1.2 GPa and 950–1000 °C. Am. Mineral. 100, 1790–1802.
McCubbin, F.M., et al., 2012. Hydrous melting of the Martian mantle produced both depleted and enriched shergottites. Geology 40, 683–686.
McCubbin, F.M., et al., 2011. Fluorine and chlorine abundances in lunar apatite: implications for heterogeneous distributions of magmatic volatiles in the lunar interior. Geochim. Cosmochim. Acta 75, 5073–5093.
McCubbin, F.M., et al., 2010a. Nominally hydrous magmatism on the Moon. Proc. Natl. Acad. Sci. USA 27, 11223–11228.
McCubbin, F.M., et al., 2010b. Detection of structurally bound hydroxyl in fluorapatite from Apollo mare basalt 15058,128 using TOF-SIMS. Am. Mineral. 95, 1141–1150.
Pahlevan, K., Stevenson, D.J., 2007. Equilibration in the aftermath of the lunar-forming giant impact. Earth Planet. Sci. Lett. 262, 438–449.
Richet, P., Bottinga, Y., Javoy, M., 1977. A review of hydrogen, carbon, nitrogen, oxygen, sulphur and chlorine stable isotope fractionation among gaseous molecules. Annu. Rev. Earth Planet. Sci. 5, 65–110.
Robinson, K.L., et al., 2014. Primitive lunar water in evolved rocks? In: 45th Lunar and Planetary Science Conference, #1607.
Saal, A.E., Hauri, E.H., Van Orman, J.A., Rutherford, M.J., 2013. Hydrogen isotopes in lunar volcanic glasses and melt inclusions reveal a carbonaceous chondrite heritage. Science 340, 1317–1320.
Sarafian, A.R., Nielsen, S.G., Marschall, H.R., McCubbin, F.M., Monteleone, B.D., 2014. Early accretion of water in the inner Solar System from a carbonaceous chondrite-like source. Science 346, 623–626.
Saxena, P., Petro, N.E., Mandell, A.M., 2016. The atmospheric evolution of magma-ocean worlds: application to the early Moon and exoplanets. In: 47th Lunar and Planetary Science Conference, #1242.
Sharp, Z.D., et al., 2013a. The chlorine isotope composition of chondrites and Earth. Geochim. Cosmochim. Acta 107, 189–204.
Sharp, Z.D., McCubbin, F.M., Shearer, C.K., 2013b. A hydrogen-based oxidation mechanism relevant to planetary formation. Earth Planet. Sci. Lett. 380, 88–97.
Sharp, Z.D., Shearer, C.K., McKeegan, K.D., Barnes, J.D., Wang, Y.Q., 2010. The chlorine isotope composition of the Moon and implications for an anhydrous mantle. Science 329, 1050–1053.
Shearer, C.K., Elardo, S.M., Petro, N.E., Borg, L.E., McCubbin, F.M., 2015. Origin of the lunar highlands Mg-suite: an integrated petrology, geochemistry, chronology, and remote sensing perspective. Am. Mineral. 100, 294–325.
Snyder, G.A., Taylor, L.A., Neal, C.R., 1992. A chemical model for generating the sources of mare basalts: combined equilibrium and fractional crystallization of the lunar magmasphere. Geochim. Cosmochim. Acta 56, 3809–3823.
Tartèse, R., et al., 2014a. Apatites in lunar KREEP basalts: the missing link to understanding the H isotope systematics of the Moon. Geology 42, 363–366.
Tartèse, R., Anand, M., Joy, K.H., Franchi, I.A., 2014b. H and Cl isotope systematics of apatite in brecciated lunar meteorites Northwest Africa 4472, Northwest Africa 773, Sayh al Uhaymir 169, and Kalahari 009. Meteorit. Planet. Sci. 49, 2266–2289.
Tartèse, R., et al., 2013. The abundance, distribution, and isotopic composition of Hydrogen in the Moon as revealed by basaltic lunar samples: implications for the volatile inventory of the Moon. Geochim. Cosmochim. Acta 122, 58–74.

Treiman, A.H., Boyce, J.W., Gross, J., Guan, Y., Eiler, J.M., 2014. Phosphate-halogen metasomatism of lunar granulite 79215: impact-induced fractionation of volatiles and incompatible elements. Am. Mineral. 99, 1860–1870.

Ustunisik, G., Nekvasil, H., Lindsley, D., 2011. Differential degassing of H_2O, Cl, F, and S: potential effects on lunar apatite. Am. Mineral. 96, 1650–1653.

Ustunisik, G., Nekvasil, H., Lindsley, D.H., McCubbin, F.M., 2015. Degassing pathways of Cl-, F-, H-, and S-bearing magmas near the lunar surface: Implications for the composition and Cl isotopic values of lunar apatite. Am. Mineral. 100, 1717–1727.

Wang, K., Jacobsen, S.B., Sedaghatpour, F., Chen, H., Korotev, R.L., 2015. The earliest Lunar Magma Ocean differentiation recorded in Fe isotopes. Earth Planet. Sci. Lett. 430, 202–208.

Warren, P.H., Wasson, J.T., 1979. The origin of KREEP. Rev. Geophys. Space Phys. 17, 73–88.

Webster, J.D., De Vivo, B., 2002. Experimental and modeled solubilities of chlorine in aluminosilicate melts, consequences of magma evolution, and implications for exsolution of hydrous chloride melt at Mt Somma-Vesuvius. Am. Mineral. 87, 1046–1061.

Webster, J.D., Kinzler, R.J., Mathez, E.A., 1999. Chloride and water solubility in basalt and andesite melts and implications for magmatic degassing. Geochim. Cosmochim. Acta 63, 729–738.

Wiechert, U., et al., 2001. Oxygen isotopes and the Moon-forming giant impact. Science 294, 345–348.

Williams, J.T., et al., in press. The chlorine isotopic composition of martian meteorites part 1: Chlorine isotope composition of martian mantle and crustal reservoirs and their interactions. Meteorit. Planet. Sci. 51.

Wing, B.A., Farquhar, J., in press. Sulfur isotope homogeneity of lunar mare basalts. Geochim. Cosmochim. Acta.